Cholesterol Supports Headgroup Superlattice Domain Formation in Fluid Phospholipid/Cholesterol Bilayers

ARTICLE *in* THE JOURNAL OF PHYSICAL CHEMISTRY B · APRIL 2006

Impact Factor: 3.3 · DOI: 10.1021/jp0558371 · Source: PubMed

9 AUTHORS, INCLUDING:

Brian Cannon
Loyola University Chicago
16 PUBLICATIONS **183** CITATIONS
SEE PROFILE

Pentti Somerharju
University of Helsinki
146 PUBLICATIONS **4,768** CITATIONS
SEE PROFILE

Juyang Huang
Texas Tech University
68 PUBLICATIONS **1,431** CITATIONS
SEE PROFILE

Kwan H Cheng
Trinity University
98 PUBLICATIONS **1,855** CITATIONS
SEE PROFILE

Cholesterol Supports Headgroup Superlattice Domain Formation in Fluid Phospholipid/Cholesterol Bilayers

Brian Cannon,[†] Anthony Lewis,[†] Jennifer Metze,[†] Visveswaran Thiagarajan,[‡] Mark W. Vaughn,[‡] Pentti Somerharju,[§] Jorma Virtanen,[⊥] Juyang Huang,[†] and Kwan Hon Cheng*[,†]

Department of Physics, Texas Tech University, Lubbock, Texas 79409-1051, Department of Chemical Engineering, Texas Tech University, Lubbock, Texas 79409, Institute of Biomedicine, University of Helsinki, Helsinki, Finland, and NanoScience Center, Department of Chemistry, University of Jyväskylä, Jyväskylä, Finland

Received: October 12, 2005; In Final Form: January 31, 2006

Fluorescence and Fourier transform infrared (FTIR) spectroscopic techniques were used to explore the effect of added cholesterol on the composition-dependent formation of putative phospholipid headgroup superlattices in fluid 1-palmitoyl-2-oleoyl-phosphatidylethanolamine/1-palmitoyl-2-oleoyl-phosphatidylcholine/cholesterol (POPE/POPC/CHOL) bilayers. Steady-state fluorescence anisotropy measurements of diphenylhexatriene (DPH) chain-labeled phosphatidylcholine (DPH-PC) revealed significant dips at several POPE-to-phospholipid mole fractions (X_{PE}'s) when the cholesterol-to-lipid mole fraction (X_{CHOL}) was fixed at 0.00, 0.35, 0.40, and 0.50. Most of the observed dips occur at or close to critical X_{PE}'s predicted by the Headgroup Superlattice (SL) model, suggesting that phospholipid headgroups of different structures tend to adopt regular distributions even in the presence of cholesterol. Time-resolved fluorescence anisotropy measurements revealed that DPH-PC senses a disordered and highly mobile microenvironment in the POPE/POPC/CHOL bilayers at those critical X_{PE}'s, indicating that this probe may partition to defect regions in the bilayers. The presence of coexisting packing defect regions and regularly distributed SL domains is a key feature predicted by the Headgroup SL model. Importantly, probe-free FTIR measurements of acyl chain C−H, interfacial carbonyl, and headgroup phosphate stretching peak frequencies revealed the presence of abrupt changes at X_{PE}'s close to those observed in the fluorescence data. When X_{PE} was varied from 0.60 to 0.72 and X_{CHOL} from 0.34 to 0.46, a clear dip at the lipid composition coordinates (X_{PE}, X_{CHOL}) ≈ (0.68, 0.40) was observed in the three-dimensional surface plots of DPH-PC anisotropy as well as the carbonyl and phosphate stretching frequencies. The critical X_{CHOL} at 0.40 agrees with the Cholesterol SL model, which assumes that cholesterol and phospholipid form SL domains at the lipid acyl chain level. In conclusion, this study provides evidence that cholesterol supports formation of phospholipid headgroup SLs in fluid state ternary lipid bilayers. The feasibility of the parallel existence of SLs at the lipid headgroup and acyl chain levels supports the relevance of the lipid SL model for the membranes of eukaryotic cells that typically contain significant amounts of cholesterol. We speculate that lipid SL formation may play a central role in the regulation of membrane lipid compositions, maintenance of organelle boundaries, and other crucial phenomena in those cells.

Introduction

The lateral organization of lipids in bilayers, particularly the formation of lipid domains and its role in the structure and function of cellular membranes, has been extensively studied in recent years.[1−5] It is now commonly believed that lipids are not randomly distributed but form compositionally distinct domains.[5−7] This lipid domain hypothesis has important implications on such crucial phenomena such as signal transduction, endo- and exocytosis, as well as intracellular lipid and protein sorting.[8−13] The mechanisms of such putative domain formation are not clear, but segregation of cholesterol and sphingolipids due to their mutual affinity/high melting temperature could be involved.[14] However, there is also evidence, mainly from model membrane studies, that the different lipid species in multicomponent membranes tend to adopt regular (even) lateral distributions.[1,7] This phenomenon, referred to as lipid superlattice (SL) formation, is intriguing since it could represent the primary "signal" or switch regulating the lipid composition of cellular membranes.[6] The formation of the putative membrane SLs is thought to be driven mainly by repulsive interactions and, perhaps surprisingly, by entropy gain.[1] Notably, the SL model and the domain segregation models are not mutually exclusive, since the SL model predicts that, at many compositions, domains with different SLs exist, and second, the sphingolipid/cholesterol domains (rafts) could have a superlattice-like organization.

Our previous fluorescence and Fourier transform infrared (FTIR) measurements have provided evidence for the formation of different SLs in fluid phosphatidylethanolamine/phosphatidylcholine (PE/PC) bilayers.[15,16] The evidence comes from abrupt changes (dips or peaks) in fluorescence or FTIR signals

* Author to whom correspondence should be addressed. Phone: (806) 742-2992. Fax: (806) 742-1182. E-mail: vckhc@ttacs.ttu.edu.
[†] Department of Physics, Texas Tech University.
[‡] Department of Chemical Engineering, Texas Tech University.
[§] University of Helsinki.
[⊥] University of Jyväskylä.

10.1021/jp0558371 CCC: $33.50
Published on Web 02/28/2006

observed at several critical compositions of PE-to-phospholipid fractions (X_{PE}) of approximately 0.10, 0.16, 0.25, 0.33, 0.50, 0.66, 0.75, 0.82, and 0.88 predicted by the Headgroup SL model. However, several studies have provided evidence for SL formation in binary cholesterol/PC bilayers[7,17] based on a similar Cholesterol SL model. However, there are no studies on ternary systems containing PC, PE, and cholesterol. Such studies would be crucial since biological membranes are much more complex than binary lipid bilayers, and second, these three lipids represent the major components of most mammalian membranes.

Here, we employed a fluorescent PC labeled with diphenylhexatriene (DPH) to the *sn*-2 acyl chain (DPH-PC) to probe the lipid SL formation in fluid PE/PC/cholesterol, or PE/PC/CHOL, ternary bilayers. Fluorescence of DPH-PC has been shown to be a sensitive indicator of bilayer packing properties.[17−21] We also carried out complementary and probe-independent FTIR studies to obtain information on the motional order of the acyl chains and the order and/or hydration of interfacial and headgroup regions as a function of bilayer composition. A recently devised low-temperature trapping (LTT) method was used to obtain compositionally uniform and fully equilibrated liposomal bilayers.[22]

We found major deviations at X_{PE}'s of approximately 0.24, 0.33, 0.50, 0.67, 0.78, and 0.84 in both DPH-PC and FTIR measurements at a fixed cholesterol-to-lipid content (X_{CHOL}), suggesting that different ternary SLs can exist in fluid PE/PC/CHOL bilayers. Also three-dimensional (3D) plots derived from both fluorescence and FTIR measurements of PE/PC/CHOL revealed a significant dip at the composition coordinates of (X_{PE}, X_{CHOL}) $\approx$ (0.68, 0.40) in agreement with the Headgroup and Cholesterol SL models. Our results provide evidence that cholesterol strongly supports headgroup superlattices and that cholesterol and headgroup SLs may coexist in fluid bilayers containing lipids of different headgroup sizes and cholesterol.

Materials and Methods

Materials. 1-Palmitoyl-2-oleoyl-PE (POPE) and 1-palmitoyl-2-oleoyl-PC (POPC) were purchased from Avanti Polar Lipids, Inc. (Alabaster, AL), and cholesterol from Nu Chek Prep, Inc. (Elysian, MN). Lipid purity (>99%) was confirmed by thin-layer chromatography on washed, activated silica gel plates (Alltech Associates, Inc., Deerfield, IL) developed with chloroform/methanol/water = 65:25:4 and petroleum ether/ethyl ether/chloroform = 7:3:3 for phospholipid and cholesterol analysis, respectively. All solvents were of HPLC grade. Fluorescently labeled PC lipid, 1-palmitoyl-2-((2-(4-(6-phenyl-*trans*-1,3,5-hexatrienyl)phenyl)ethyl)carbonyl)-3-*sn*-PC (DPH-PC), was obtained from Molecular Probes (Eugene, OR). DPH-PC consists of a 16-carbon saturated fatty acyl chain attached to the *sn*-1 position of the glycerol backbone and a diphenylhexatriene (DPH) fluorophore attached to the *sn*-2 position of the same glycerol backbone via a short propanoyl chain of a PC molecule. Concentrations of all phospholipid stocks in chloroform were determined by a phosphate assay.[23] Aqueous buffer (pH 7.0, 5 mM PIPES, 200 mM KCl, 1 mM NaN_3) was prepared from deionized water (~18 MΩ) and filtered through a 0.1μm filter before use.

Preparation of POPE/POPC/CHOL Liposomes. Compositionally uniform POPE/POPC/CHOL liposomes containing 0.1 mol % of DPH-PC were prepared using aLTT technique.[17,21] The total amount of lipids in each sample was 0.2 μmol. LTT produces homogeneous and compositionally uniform liposomes even at high cholesterol contents, which is particularly important in the present context. The samples were stored at 23 °C in the dark in a mechanical shaker for at least 10 days and vortexed vigorously once a day before fluorescence measurements to ensure phase equilibrium. Previous X-ray diffraction measurements on POPC/CHOL or POPE/CHOL liposomes prepared by this LTT method showed no cholesterol precipitation within the range of X_{CHOL} used here.[22] TLC analysis revealed no degradation of the lipids during the equilibration period.

Steady-State and Time-Resolved Fluorescence Measurements of DPH-PC. Steady-state fluorescence anisotropy (r) measurements of DPH-PC in POPC/CHOL mixtures were performed at 23 °C on either a GREG-PC (ISS, Inc., Champaign, IL) fluorimeter or a QuantaMaster C61/2000 spectrofluorimeter (PTI, Inc., Lawrenceville, NJ) using a T-mode single-photon-counting configuration.[24] Briefly, a Liconix 4240 NB continuous wave He−Cd UV laser (Santa Clara, CA) emitting at 325 nm or a 200 W xenon arc lamp with the monochromator set at 310 nm (4 nm slit) was used for excitation with the ISS or PTI instrument, respectively. Two 350 nm cutoff filters or two emission monochromators set at 430 nm with 6 nm slit widths for the ISS or PTI instrument, respectively, were used to collect the fluorescence emission. Here, r is defined as $(I_{||} - gI_{\perp})/(I_{||} + 2gI_{\perp})$, where $I_{||}$ or $I_{\perp}$ are the photon counts from the parallel or perpendicular polarization emission, respectively, and g is the g-factor related to the relative sensitivity of the two emission channels and can be obtained when the excitation polarization is set to perpendicular.[20,24] The integration time of the detectors was usually set at 0.5 s, and 20 repeats were averaged. The sample was under constant stirring during the measurements. Comparable results were obtained from both ISS and PTI instruments.

Time-resolved anisotropy decay $r(t)$ measurements of DPH-PC were obtained using a QuantaMaster C61/2000 spectrofluorimeter (PTI Inc., Lawrenceville, NJ) equipped with a fluorescence lifetime subsystem using a pulsed nitrogen laser emitting at 334 nm. A stroboscopic optical boxcar detection technique [25] was used for time-resolved data collection. Briefly, two parallel and perpendicular intensity decays, i.e., $I_{||}(t)$ and $I_{\perp}(t)$, respectively, were measured simultaneously from each fluorescent sample upon a parallel-polarized laser excitation using a T-mode configuration. A deconvolution of the raw decay signals with the impulse−response signals of the two detectors was also performed. The impulse−response signals were determined by replacing the fluorescent sample with a nonfluorescent scattering solution made of glycogen in water. The anisotropy decay $r(t)$ is then defined as $(I_{||}(t) - gI_{\perp}(t))/I(t)$, where g is the g-factor similar to the steady-state g-factor described above but is calculated by taking the ratio of the integrated intensity of the perpendicular decay to that of the parallel decay of the fluorescent sample using a perpendicular-polarized laser excitation. $I(t)$ represents the total intensity decay and is defined as $(I_{||}(t) + 2gI_{\perp}(t))$.

Some $r(t)$ and $I(t)$ decay measurements were performed in the frequency domain[24,26] on an ISS GREG 200 (ISS, Inc., Champaign, IL) fluorometer equipped with digital multifrequency cross-correlation phase and modulation acquisition electronics. A He−Cd laser was used as the excitation source. The frequency-domain measurements and data analysis have been described in detail elsewhere.[15,17,20,24] Comparable time-resolved results were obtained from both time-domain PTI and frequency-domain ISS instruments.

Time-Resolved Fluorescence Data Analysis. The fluorescence intensity decay $I(t)$ of DPH-PC can be described by a double-exponential decay function using eq 1

$$I(t) = \sum_{i=1}^{2} \alpha_i \, e^{-t/\tau_i} \quad (1)$$

In the double-exponential fits, the long and short fluorescence decay lifetime components are indicated by τ_1 and τ_2, respectively. The molar fractions of the long and short components are defined as α_1 and α_2, respectively. The intensity-weighted averaged fluorescence lifetime $\langle\tau\rangle$ can be calculated from $f_1\tau_1 + f_2\tau_2$, where f_i is the intensity fraction of the ith component and can be expressed as $\alpha_i\tau_i/(\alpha_1\tau_1 + \alpha_2\tau_2)$.[17,24]

A wobbling diffusion model[27,28] was used to fit the anisotropy decay $r(t)$ data. The initial anisotropy r_0, order parameter S, and rotational diffusion rate D of DPH-PC in lipid bilayers were obtained using eq 2

$$r(t) = r_0[(1 - S^2)\, e^{-6Dt/(1-S^2)} + S^2] \quad (2)$$

In general, the initial anisotropy r_0, i.e., the anisotropy of the fluorophore at time zero after excitation, is a constant, which depends on the relative orientation of the absorption and emission dipoles of the probe.[20] In this study, its value is fixed at 0.34 based on the previous results[20] for simplicity in the data analysis. The order parameter S, which may vary from 0 to 1, describes the orientational order of the DPH probe relative to the normal of the lipid bilayers.[20] The localized rotational diffusion constant D describes the rate of wobbling diffusion of the probe among the acyl chains of the matrix lipid. With this notation, a diminished value of S or an increase in D may be interpreted as an increased disorder (e.g., due to bilayer packing defects) of the local environment of DPH-PC in the host lipid bilayer.

It is important to mention that the steady-state anisotropy r is related to $I(t)$ and $r(t)$ according to eq 3[27]

$$r = \frac{\int_0^\infty r(t)\, I(t)\, dt}{\int_0^\infty I(t)\, dt} \quad (3)$$

Therefore, r contains information for the fluorescence decay and rotational dynamics components.

A rotation correlation time ρ can also be used to quantify the rotational mobility of the fluorescent probe in the bilayer. This parameter is inversely proportional to the average rotational rate of the probe and can be calculated from the values of measured values of $\langle\tau\rangle$ and r as described by eq 4[15,29]

$$\rho = \frac{\langle\tau\rangle}{(r_0/r - 1)} \quad (4)$$

FTIR Measurements. POPE/POPC/CHOL liposomes were prepared as for fluorescence measurements, except that the total amount of lipid was 0.8 μmol and no DPH-PC was included. After preparation and >10 days of equilibration at 23 °C, the liposomes were pelleted by centrifugation at 20 000g for 20 min at 23 °C and then applied on a single reflection horizontal attenuated total reflectance (ATR) sample cell (Pike Technologies, Inc., Madison, WI) at 23 °C. The infrared spectra were recorded with a Magna-IR 560 FTIR spectrometer (Nicolet, Inc., Madison, WI) equipped with a deuterated triglycine sulfate detector operated at room temperature. Typically, 50 interferograms with 1 cm^{-1} resolution were collected, averaged, Fourier transformed, and subtracted from the background using standard procedures[30] with the Omni Software provided by Nicolet. The contributions of water and cholesterol were also subtracted based on the published procedures.[17,31,32] To reduce noise, each subtracted spectrum was smoothed by a fifth-degree polynomial filtering mask using the Savitzky−Golay algorithm.[33] The peak positions of the smoothed spectra were subsequently determined using the peak picking routine using the same sensitivity and threshold for all lipid vibrational bands, antisymmetric O═P═O, C═O, and symmetric C−H.[17] The Savitzky−Golay filtering and peak picking software routines were provided by Omni.

Data Smoothing. Our raw data sets (P_{ij}) consisted of fluorescence or FTIR spectroscopic parameters as a function of lipid composition (j) measured from several parallel sample sets (i), each independently prepared by the LTT method. In this study, the major lipid composition variable refers to the PE-to-total phospholipid (PE + PC) mole ratio (X_{PE}) or the cholesterol-to-total lipid mole ratio (X_{CHOL}). The primary data set consisted of averages ($\bar{P}_j$) of data from parallel sample sets as shown in eq 5

$$\bar{P}_j = \sum_{i=1}^{n} [P_{ij}]\left[\frac{1}{n}\right] \quad (5)$$

Here n is the total number of parallel samples from independent sample sets. Additional smoothed data sets and one-pass ($\bar{P}_j^1$) and two-pass ($\bar{P}_j^2$) multipoint running averages were subsequently generated. For the case of three-point running averages, these one-pass or two-pass running averages are identical to applying data filtering masks of (1/3, 1/3, 1/3) or (1/9, 2/9, 3/9, 2/9, 1/9) to 3 and 5 consecutive raw data point sequences, respectively, as shown in eqs 6 and 7

$$\bar{P}_j^{\,1} = \sum_{i=1}^{n}\left[\frac{P_{ij-1} + P_{ij} + P_{ij+1}}{3}\right]\left[\frac{1}{n}\right] \quad (6)$$

$$\bar{P}_j^{\,2} = \sum_{i=1}^{n}\left[\frac{P_{ij-2} + 2P_{ij-1} + 3P_{ij} + 2P_{ij+1} + P_{ij+2}}{9}\right]\left[\frac{1}{n}\right] \quad (7)$$

However, the masks for the case of two-point running averages are (1/2, 1/2) or (1/4, 1/2, 1/4), respectively, as shown in eqs 8 and 9

$$\bar{P}_j^{\,1} = \sum_{i=1}^{n}\left[\frac{P_{ij-1} + P_{ij}}{2}\right]\left[\frac{1}{n}\right] \quad (8)$$

$$\bar{P}_j^{\,2} = \sum_{i=1}^{n}\left[\frac{P_{ij-1} + 2P_{ij} + P_{ij+1}}{4}\right]\left[\frac{1}{n}\right] \quad (9)$$

Overall, this multiple-pass data smoothing protocol[34] serves the purpose of suppressing data scatter due to random errors of spectroscopic measurements and sample preparation. However, a drawback of such a filtering procedure is that it might suppress small (but real) deviations determined by one or two data points only. The smoothed data sets $\bar{P}_j^1$ and $\bar{P}_j^2$ were used to reduce noise and help locate any dips, peaks, or other deviations in the primary data plots, e.g., $\bar{P}_j$ versus X_{PE}. Because of the use of multipoint running averages, only the deviations defined by two or more primary data points were considered significant. For the steady-state fluorescence parameter set with an X_{PE} increment of 0.01, the three-point running averages were used. However, for the FTIR parameter set with an X_{PE} increment of 0.02, the two-point running averages were used instead. Through the use of these smoothing protocols, the X_{PE} composition range of data averages is exactly 0.04 for both fluorescence and FTIR parameters.

Statistical Significance of Deviations. The statistical significance of the peaks and dips in the measured spectroscopic parameter versus X_{PE} or X_{CHOL} plots was analyzed using an unidirectional *t*-test of unequal variances.[35] The *t*-test allows one to assess whether the means of two different groups of measurements are statistically different from each other. In this study, the two means represented the mean of the peak or dip (P_c) at the critical PE or cholesterol composition and the mean of the adjacent or baseline value (P_b) at the nearby composition content obtained from independently prepared parallel samples. The standard deviations, σ_c and σ_b, and sample sizes, n_c and n_b, for the critical and baseline values were also needed. From the above statistical parameters, a *t*-value[35] was calculated as shown in eq 10

$$t = \frac{|P_c - P_b|}{\sqrt{\frac{\sigma_c^2}{n_c} + \frac{\sigma_b^2}{n_b}}} \tag{10}$$

The probability (*p*-value) of accepting the null hypothesis of the two means being identical, i.e., $P_c = P_b$, was obtained from the *t*-distribution with the degree of freedom given by $n_c + n_b - 2$.[17,35,36] The probability of rejecting the null hypothesis, or probability of significance of the difference of the two means, is then defined as $(1 - p) \times 100\%$. In our case, the statistical significance of the peak or dip value as compared with two baseline values is represented by two numbers, P_L and P_R, where P_L or P_R represents the probability that the value of a dip (or peak) is different from the adjacent starting (left) and ending (right) sides of the dip (or peak), respectively, along the composition axis based on the *t*-test. Raw P_{ij}, instead of averaged or smoothed, data sets were used in all statistical analysis.[17] Peaks or dips with both P_L and P_R less than 70% were ignored. Although the 70% cutoff is arbitrary, the values of P_L and P_R provide a standard gauge to examine and cross-compare the critical changes of the spectroscopic parameters.

Molecular Organization of the Cholesterol/Phospholipid Bilayer at Both Acyl Chain and Headgroup Levels. The current SL model predicts that lipid mixtures tend to adopt regular SL-like lateral distributions at either the acyl chain level or headgroup level.[1,7] Interestingly, there are only a finite number of allowed critical compositions of each component that may form SL structures. These critical or SL compositions can readily be obtained from eq 11

$$x_g = \frac{h}{P + h - g} \tag{11}$$

Here, x_g denotes the critical guest lipid mole fraction, P is the size of the unit cell, and h and g represent the number of lattice sites occupied by host and guest lipids, respectively. When x_g is greater than 0.5, the guest becomes the host, and the critical compositions are simply $(1 - x_g)$. As shown in Figure 1, each unit cell of a binary SL has P lattice sites with one guest molecule at the origin of the principal axes u and v. Also, the value of P depends on the symmetry of the packing, hexagonal (HX), center rectangular (CR), or rectangular (R), and on the lattice coordinates (a, b) that define the distances between two proximal guest molecules along the principal axes u and v.

In acyl chain region, where the SL contains both cholesterol and phospholipid, cholesterol is the guest ($g = 1$) and the phospholipid ($h = 2$) is the host. The critical mole fraction corresponding to a HX, CR, or R symmetric SL at the acyl chain level of the lipid bilayers, i.e., X_{CHOL}^{HX}, X_{CHOL}^{CR}, or X_{CHOL}^{R}, is given by $2/(a^2 + ab + b^2 + 1)$, $2/(1 + 2ab + b^2)$, or $2/((1 + ab + b^2)/2)$, respectively.[17] Similarly, for the case of headgroup SLs, the guest ($g = 1$) or host ($h = 1$) can be either one of the two PLs, and the critical mole fractions for the HX, CR, or R symmetric SL, i.e., X_{HG}^{HX}, X_{HG}^{CR}, or X_{HG}^{R}, are given by $1/(a^2 + ab + b^2)$, $1/(2ab + b^2)$, and $1/((ab + b^2)/2)$, respectively.[16]

Other structural models of lipid organization in cholesterol−phospholipid bilayers have also been proposed in a previous

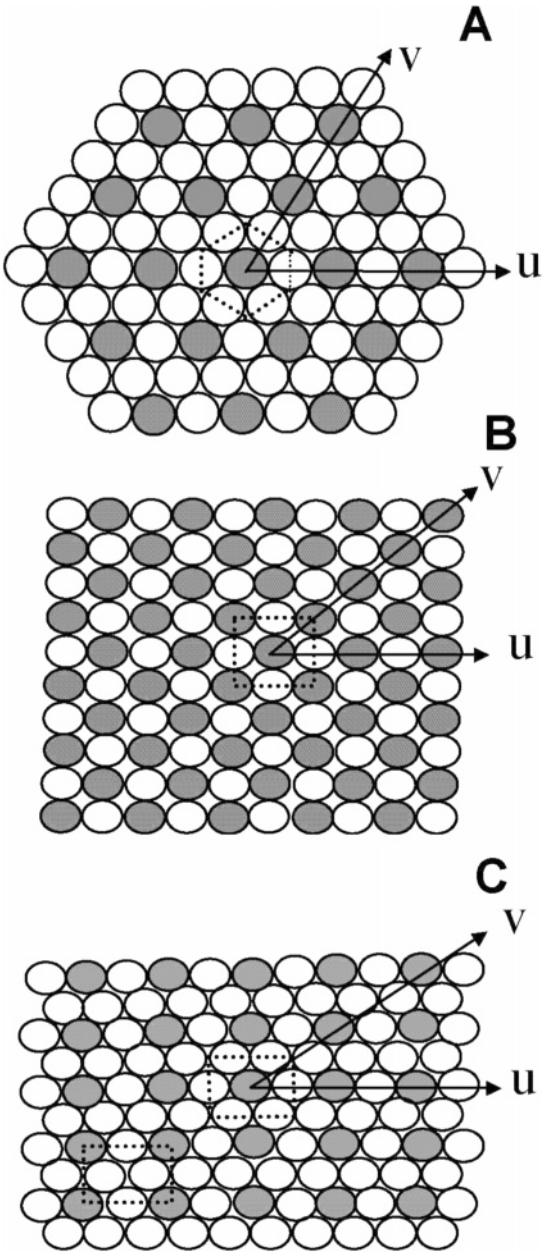

Figure 1. Molecular organizations of hexagonal, center rectangular, and rectangular superlattices. The principal axes u and v and the (a, b) lattice coordinate systems for some epresentative (A) hexagonal, (B) center rectangular, and (C) rectangular superlattices are shown. The dark circle represents the guest molecule, and the open circle the host molecule. For the headgroup superlattice, the guest or host represents one phospholipid headgroup from PC or PE. For the cholesterol SL, the guest is cholesterol and the host is one of the two acyl chains of the PC or PE. Here, the lattice coordinates are (0, 2), (1, 1), and (1, 2) for the hexagonal, center rectangular, and rectangular lattices, respectively. The unit cell for each lattice is also shown. For the case of the rectangular lattice, a unit cell with the guest either in the center or on the four corners is shown.

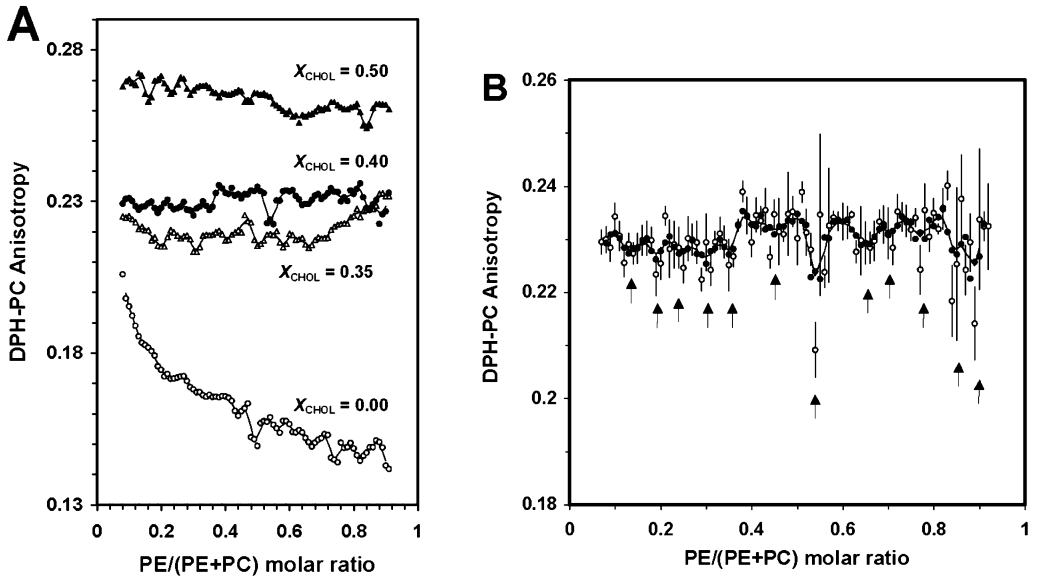

Figure 2. Steady-state anisotropy of DHP-PC in POPE/POPC/CHOL bilayers versus X_{PE}. (A) Steady-state fluorescence anisotropy of the DPH-PC plot at 23 °C for a fixed cholesterol-to-lipid mole ratio (X_{CHOL}) of 0.00 (○), 0.35 (△), 0.40 (●), and 0.50 (▲). For clarity, the data points represent the one-pass three-point running averages, and the lines denote the two-pass three-point running averages (see eqs 4−5 of the Materials and Methods section). All sample sets were equilibrated at 23 °C for at least 10 days after the LTT liposome preparation. (B) Steady-state fluorescence anisotropy of the DPH-PC plot at 23 °C for a fixed X_{CHOL} of 0.40. Raw averaged data from parallel samples (○), one-pass three-point running averages (●) and two-pass three-point running averages (line) are presented. The arrows indicate the identified deviations or dips, which are defined by at least two raw data points (see Materials and Methods section). Bars indicate standard errors.

study by Martin and Yeagle.[37] These models suggest the formation of cholesterol dimer in phospholipid bilayers at low cholesterol content, i.e., $X_{CHOL} < 0.50$, and predict abrupt changes in the membrane properties at the critical cholesterol mole fraction of 0.31 or 0.47. However, recent experimental and computer simulation studies indicated that the general behavior of cholesterol is probably more consistent with cholesterol staying in a monomer form for $X_{CHOL} < 0.50$.[38] Interestingly, at a high cholesterol mole fraction, i.e., $X_{CHOL} > 0.50$, a recent computer simulation study based on an umbrella model does predict the formation of a large-scale cholesterol dimer pattern in cholesterol−phospholipid bilayers at the critical cholesterol mole fraction of 0.57.[22] In addition, the existence of this cholesterol critical fraction of 0.57 was confirmed by our recent fluorescence anisotropy and fluorescence resonance energy transfer (FRET) experiments.[21]

Results

Steady-State Fluorescence Anisotropy Measurements. Figure 2A shows the steady-state fluorescence anisotropy (r) of DHP-PC as a function of PE-to-(PE + PC) mole ratio (X_{PE}) in ternary mixtures of POPE/POPC/CHOL with a fixed cholesterol-to-total lipid (X_{CHOL}) equal to 0, 0.35, 0.40, or 0.50. Both one-pass and two-pass running averages (see eqs 6 and 7 in the Materials and Methods section) are shown. The overall shapes of r versus X_{PE} plots were significantly affected by the amount of cholesterol present, as was the value of r. More interestingly, however, deviations (dips) were observed at each fixed X_{CHOL}. When no cholesterol was present ($X_{CHOL} = 0.00$), dips at X_{PE} of ≈ 0.44, 0.50, 0.57, 0.67, 0.75, and 0.82 were seen. For X_{CHOL} of 0.35, dips were observed at $X_{PE} \approx 0.20$, 0.31, 0.41, 0.50, 0.58, and 0.66, for X_{CHOL} of 0.40 at $X_{PE} \approx$ 0.13, 0.19, 0.24, 0.30, 0.35, 0.45, 0.54, 0.66, 0.70, 0.77, 0.85, and 0.89, and for X_{CHOL} of 0.50 at $X_{PE} \approx 0.16$, 0.23, 0.30, 0.41, 0.47, 0.64, 0.78, and 0.84. Note that for X_{CHOL} of 0.50 the dip at X_{PE} of 0.64 is much broader than the other dips at this and other cholesterol contents. A compilation of the above anisotropy dips as well as the critical X_{PE}'s, i.e., X^{HX}_{HG}, X^{CR}_{HG}, and X^{R}_{HG}, predicted by the Headgroup SL model are shown in Table 1.

TABLE 1: Comparison of Critical Mole Fractions X_{PE} from Steady-State Fluorescence Measurements of DPH-PC with X^{HX}_{HG}, X^{CR}_{HG}, or X^{R}_{HG} Values Predicted by the Headgroup SL Model for Ternary Mixtures of POPE/POPC/Cholesterol at a Fixed Cholesterol/Lipid Ratio of X_{CHOL} = 0.0, 0.35, 0.40, and 0.50[a]

X^{HX}_{HG}, X^{CR}_{HG}, or X^{R}_{HG}	X_{CHOL} = 0.00	X_{CHOL} = 0.35	X_{CHOL} = 0.40	X_{CHOL} = 0.50
$0.04-0.10^{H,CR,R}$				
$0.11-0.13^{H,CR,R}$			0.13	
$0.14^{H,CR}$, 0.17^{R}				0.16
0.20^{CR}		0.20	0.19	
$0.25^{H,CR,R}$	0.24		0.24	0.23
$0.33^{H,CR}$	0.34	0.31	0.30, 0.35	0.30
	0.44[b]	0.41[b]	0.45[b]	0.41[b]
0.50^{R}	0.49	0.50		0.47
	0.57[b]	0.58[b]	0.54[b]	
$0.67^{H,CR}$	0.67	0.66	0.66	0.64
			0.70[b]	
$0.75^{H,CR,R}$	0.75		0.77	0.78
0.80^{CR}				
0.83^{R}, $0.86^{H,CR}$	0.82		0.85	0.84
$0.87-0.89^{R,CR,H}$			0.89	
$0.92-0.96^{R,CR,H}$				

[a] The critical mole fractions are identified from the dips of the two-pass three-point running averages of the raw data (see the Materials and Methods section). Superscripts H, CR, and R denote X^{HX}_{HG}, X^{CR}_{HG}, or X^{R}_{HG}, respectively, from the Headgroup SL model. [b] Critical mole fractions that do not agree (±0.03) with X^{HX}_{HG}, X^{CR}_{HG}, or X^{R}_{HG} values.

Figure 2B shows a more detailed plot of r of DHP-PC as a function of X_{PE} in ternary mixtures of POPE/POPC/CHOL with a fixed X_{CHOL} equal to 0.40. The raw averaged data from parallel samples as well as the subsequent one-pass and two-pass three-point running averages are shown. The values of r were confined to 0.20 and 0.24, and dips of various depths were observed in the running averaged data at several locations of X_{PE}. The levels of statistical significance of each dip as compared with the left and right baseline values, i.e., (P_L, P_R), were also tabulated (see the Materials and Methods section) and shown in Table 2.

TABLE 2: Comparison of Critical Mole Fractions X_{PE} from Steady-State Fluorescence Measurements of DPH-PC and FTIR Measurements with X^{HX}_{HG}, X^{CR}_{HG}, or X^{R}_{HG} Values Predicted by the Headgroup SL Model for Ternary Mixtures of POPE/POPC/Cholesterol at a Fixed Cholesterol/Lipid Ratio of 0.40[a]

X^{HX}_{HG}, X^{CR}_{HG}, or X^{R}_{HG}	DPH-PC(P_L, P_R)	ν_{C-H} (P_L, P_R)	$\nu_{C=O}$ (P_L, P_R)	$\nu_{O=P=O}$ (P_L, P_R)
$0.04-0.08^{H,CR,R}$		0.09 (79, 85)		
$0.11-0.13^{H,CR,R}$				
$0.14^{H,CR}$, 0.17^{R}	0.13 (97, 89)		0.15 (94, 92)	0.14 (84, 80)
0.20^{CR}	0.19 (93, 93)	0.22 (84, 79)		0.21 (82, 88)
$0.25^{H,CR,R}$	0.24 (90, 83)		0.26 (68, 92)	
$0.33^{H,CR}$	0.30 (93, 94)	0.31 (91, 97)		0.32 (87, 81)
	0.35 (92, 99)			
	0.45[b] (98, 94)			
0.50^{R}		0.50 (85, 74)	0.48 (97, 96)	0.53 (77, 73)
	0.54[b] (93, 90)	0.56[b] (65, 82)	0.54[b] (95, 87)	
			0.62[b] (95. 87)	
$0.67^{H,CR}$	0.66 (92, 91)	0.66 (92, 75)	0.68 (77, 99)	0.68 (97, 99)
	0.70[b] (80, 92)			
$0.75^{H,CR,R}$	0.77 (94, 95)			
0.80^{CR}		0.78 (70. 87)		
0.83^{R}, $0.86^{H.CR}$	0.85 (86, 88)	0.83 (83, 97)		0.84 (96, 82)
$0.87-0.89^{R,CR,H}$	0.89 (81, 82)			
$0.92-0.96^{R,CR,H}$		0.96 (99, 70)		

[a] The probability of significance (P_R, P_L) of each critical mole fraction based on the *t*-test (see the Materials and Methods section) is also shown. [b] See the footnote of Table 1 for details.

Among all the identified anisotropy dips, the one at $X_{PE} \approx 0.66$ appears to be the most notable or best defined dip, which is identified by five raw data points as shown in Figure 2B. However, the dip at $X_{PE} \approx 0.45$ is rather broad, weak, and less defined and is identified by the smoothed data within a large region of $X_{PE} = 0.40-0.50$.

The observed critical X_{PE}'s that do not agree (± 0.03) with the predicted X^{HX}_{HG} and X^{CR}_{HG} were found at $X_{PE} \approx 0.44$ and 0.57 for $X_{CHOL} = 0.00$, $X_{PE} \approx 0.41$ and 0.58 for $X_{CHOL} = 0.35$, $X_{PE} \approx 0.45$, 0.54, and 0.70 for $X_{CHOL} = 0.40$, and $X_{PE} \approx 0.41$ for $X_{CHOL} = 0.50$ as shown in Table 1.

FTIR Measurements. FTIR measurements were performed on POPE/POPC/CHOL bilayers (without DPH-PC) as a function of X_{PE} at a fixed X_{CHOL} of 0.40. The phospholipid C−H, C═O, and O═P═O vibrational peak frequencies were determined after subtraction of the cholesterol's contribution [31] to the CH signal.[17,31] Figure 3 shows the C−H, C═O, and O═P═O vibrational peak frequencies as a function of X_{PE}. Raw averaged data as well as one-pass and two-pass two-point running averages (eqs 8 and 9 in the Materials and Methods section) are shown. The values of C−H, C═O, and O═P═O peak frequencies varied over a range of 2850−2851, 1732−1737, and 1220−1227 cm^{-1}, respectively. By comparison of the critical changes of the FTIR frequency data with the predicted critical compositions from the SL model, significant peaks at $X_{PE} \approx 0.09$, 0.22, 0.31, 0.50, 0.56, 0.66, 0.78, 0.83, and 0.96 were noted in the C−H versus X_{PE} plot (Figure 3A). Analogous plots for C═O and O═P═O vibrational peak frequencies show dips at $X_{PE} \approx 0.15$, 0.26, 0.48, 0.54, 0.62, and 0.68 for the C═O (Figure 3B) and at $X_{PE} \approx 0.14$, 0.21, 0.32, 0.53, 0.68, and 0.84 for O═P═O (Figure 3C). Table 2 summarizes the deviations observed in the FTIR plots and compares them with the critical X_{PE} values as predicted by the Headgroup SL model. Here most of the observed X_{PE}'s, except those at 0.53 from C−H and 0.54 and 0.62 from C═O, agree (± 0.03) with those predicted by the Headgroup SL model. For the case of O═P═O, the dip at $X_{PE} \approx 0.68$ represents the most significant dip, which is defined by eight raw data points, among all the FTIR peak frequencies measured.

Figure 4 displays the effect of cholesterol content on the vibrational frequencies of C−H, C═O, and O═P═O at a fixed X_{PE} of 0.68. Significant dips at X_{CHOL} of 0.42 and 0.40 were observed in the C═O and O═P═O plots (Figures 4B and 4C), respectively, while no clear deviations were visible in the C−H frequency versus X_{CHOL} plot (Figure 4A).

Time-Resolved Fluorescence Measurements. The total intensity decay curve $I(t)$ of DPH-PC in POPE/POPC/CHOL bilayers at different PE contents but at a fixed $X_{CHOL} = 0.40$ and at different cholesterol contents but at a fixed X_{PE} of 0.68 were obtained using the time-domain and pulsed-laser-based PTI fluorimeter (see the Materials and Methods section). Each time-domain $I(t)$ curve was subsequently fitted with a double-exponential decay function as shown in eq 1, and the fluorescence decay parameters, i.e., long (τ_1) and short (τ_2) decay lifetimes, mole fraction of the short decay component α_2, and intensity-averaged fluorescence decay lifetime ($\langle\tau\rangle$), were calculated (see the Materials and Methods section) using a nonlinear regression procedure.[17,20] Figure 5 shows the representative recovered fluorescence decay parameters from one of the three independently prepared sample sets. For the case of different PE contents at a fixed X_{CHOL} of 0.40, the long and short decay components are well resolved as shown in Figure 5A. These two decay lifetimes decreased with X_{PE} content. The value of α_2 exhibited a minimum at $X_{PE} \approx 0.68$ as shown in Figure 5B. No significant change was found for the average lifetime as shown in Figure 5A. For the case of different cholesterol content at a fixed X_{PE} of 0.68, the long and short decay components are also clearly resolved as shown in Figure 5C. A prominent dip at $X_{CHOL} \approx 0.40$ was observed for both τ_1 and τ_2. The value of α_2 also exhibited a dip at $X_{CHOL} \approx 0.40$ as shown in Figure 5D. No significant change was again found for the average lifetime as shown in Figure 5C. Similar trends were observed for samples from different preparations. Some frequency-domain intensity decay measurements using the ISS fluorimeter (see the Materials and Methods section) were also performed (results not shown) on some PE/PC/CHOL ternary mixtures, and results were similar to those using the PTI fluorimeter as mentioned above.

The anisotropy decay curves $r(t)$ of DPH-PC in POPE/POPC/CHOL bilayers at different PE contents but at a fixed X_{CHOL} of 0.40 (Figure 6) and at different cholesterol contents but at a fixed X_{PE} of 0.68 (Figure 7) were also obtained using the PTI fluorimeter. Subsequently, orientational dynamics parameters of DPH-PC, i.e., rotational correlation time ρ, order parameter S, and diffusion constant D (see eqs 2 and 4 in the Materials and Methods section), were determined from the $r(t)$ curves

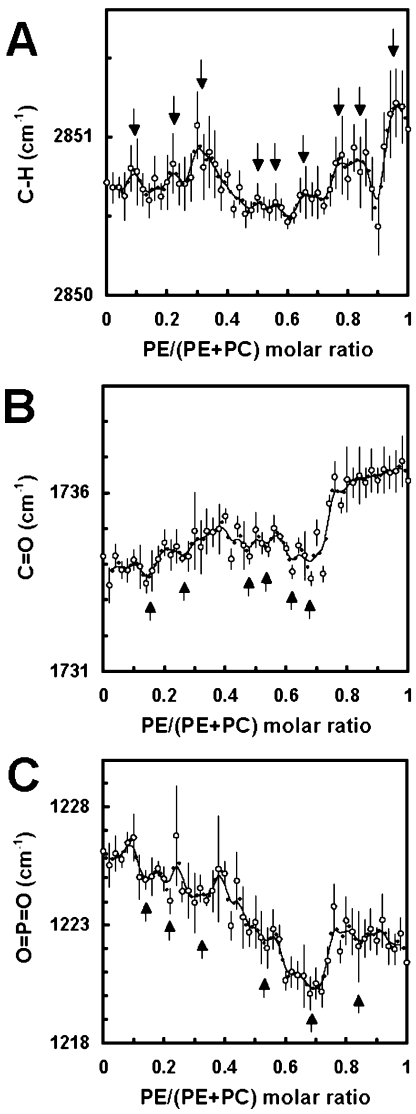

Figure 3. Peak of the FTIR vibrational frequency band of (A) C−H, (B) C═O, and (C) O═P═O of phospholipids in POPE/POPC/CHOL bilayers as a function of X_{PE}. The FTIR measurements were carried out at 23 °C for $X_{CHOL} = 0.40$. See the legends of Figure 2B for other details. For the case of C−H (A), the arrows indicate the peaks instead of dips in the plot.

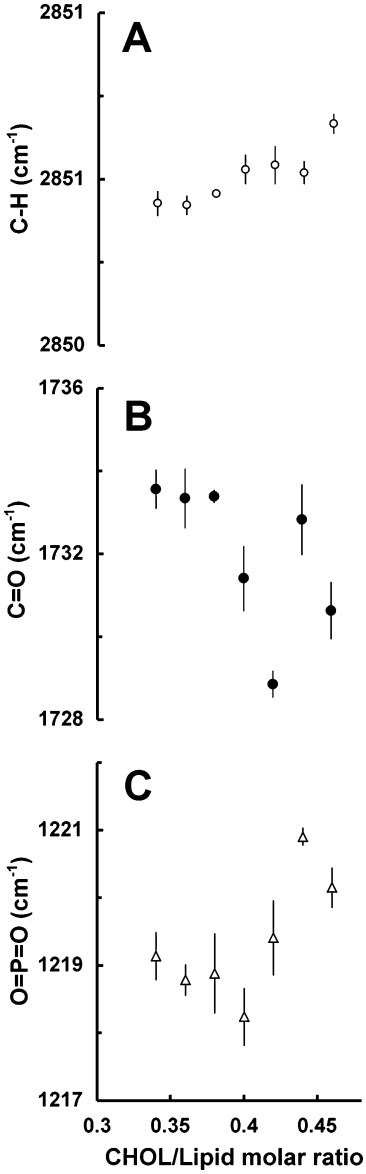

Figure 4. Peak of the FTIR vibrational frequency band of (A) C−H, (B) C═O, and (C) O═P═O of phospholipids in POPE/POPC/CHOL bilayers as a function of X_{CHOL}. The FTIR measurements were carried out at 23 °C for $X_{PE} = 0.67$. See the legends of Figure 2B for other details.

using a nonlinear regression analysis procedure.[17,20] For the purpose of comparison, the steady-state anisotropy *r* plots were also shown. For the case of different PE contents at a fixed $X_{CHOL} = 0.40$, a dip in rotational correlation time (Figure 6B), a dip in order parameter (Figure 6C), and a peak in diffusion constant (Figure 6D) at $X_{PE} = 0.68$ were observed. These results indicated a decrease in the orientational order and an increase in the rotational rate of DPH in the lipid matrix of POPE/POPC/CHOL at the critical X_{PE} of 0.68. These critical changes in the time-resolved orientational dynamics parameters at $X_{PE} = 0.68$ agreed with the dip at the same X_{PE} of 0.68 in the steady-state anisotropy plot (Figure 6A). As shown in Figure 7, similar observations in the deviations of the orientational dynamics parameter versus composition plots were found but at $X_{CHOL} = 0.40$ for the case of different cholesterol contents but at a fixed X_{PE} of 0.68. Again, the anisotropy decay measurements[20] using the ISS fluorimeter agreed favorably with those using the PTI fluorimeter (results not shown).

Three-Dimensional Plots Supporting the Existence of Abrupt Changes at (X_{PE}, X_{CHOL}) ≈ (0.67, 0.40). Steady-state fluorescence spectroscopy and FTIR were used to further study the physical state of the bilayer when the PE and cholesterol mole fractions were varied systematically from 0.60 to 0.72 and from 0.34 to 0.46, respectively. To generate 3D surface plots, i.e., spectroscopic data versus two-dimensional composition coordinates (X_{PE}, X_{CHOL}), a two-dimensional Gaussian smoothing mask (3 pixels in width, 1 pixel sigma) was applied to the raw data using image processing software Transform 3.3 (Fortner Software, Inc., Sterling, VA). This postimage processing procedure is routinely used in radiation dosimetry calibration to visualize 3D or volume imaging data.[39] Here the 3D surface plot of the steady-state anisotropy of DPH-PC (Figure 8A) revealed a local dip in the composition coordinates of (X_{PE}, X_{CHOL}) ≈ (0.67, 0.41). Figures 8B and 8C show the surface plots of the calculated order parameter (Figure 8B) and diffusion constant (Figure 8C) of DPH-PC in which a local minimum and a local maximum in the composition coordinates of (X_{PE}, X_{CHOL}) ≈ (0.68, 0.40) were found. Similar 3D surface plots of the FTIR peak frequencies are shown in Figure 9. A local dip

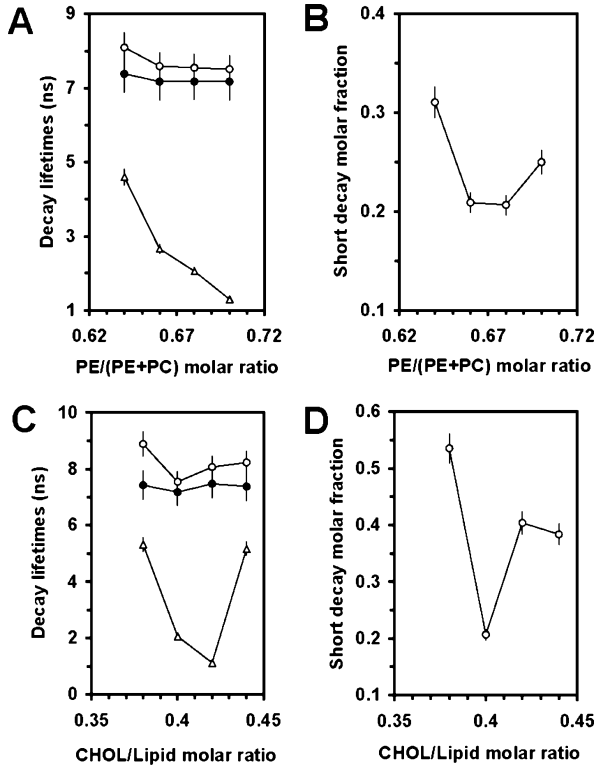

Figure 5. Time-resolved fluorescence intensity decay parameters of DPH-PC in POPE/POPC/CHOL bilayers as a function of X_{PE} at a fixed $X_{CHOL} = 0.40$ or as a function of X_{CHOL} at a fixed $X_{PE} = 0.68$. The resolved long component (○), short component (△), and intensity-averaged (●) fluorescence decay lifetime (●) for a fixed $X_{CHOL} = 0.40$ (A) or a fixed $X_{PE} = 0.68$ (C) are shown. The short decay mole fraction for a fixed $X_{CHOL} = 0.40$ (B) or a fixed $X_{PE} = 0.68$ (D) are also shown. The uncertainties of the fitted parameters obtained from three independent samples are indicated by error bars.

at (X_{PE}, X_{CHOL}) ≈ (0.67, 0.42) for C═O and at (X_{PE}, X_{CHOL}) ≈ (0.67, 0.40) for O═P═O were also revealed.

Discussion

The present study provides new spectroscopic evidence that regular, superlattice-like arrangements at certain critical lipid compositions in phospholipid bilayers exist at the headgroup and acyl chain levels for fluid state PE/PC/cholesterol. The observed critical compositions agree favorably with the Headgroup and Cholesterol Superlattice models.[1,6,7] Since PE, PC, and cholesterol are major lipid components of mammalian cell membranes, the existence of superlattice-like domains at both the headgroup and the acyl chain levels could be involved in the regulation of lipid compositions [1,6] and other lipid domain-mediated membrane activities.[3,8,9,12,13,40,41]

Previous studies employing various fluorescent probes and probe-independent FTIR[15,16] have suggested that SL domains form in binary PE/PC bilayers. In separated but similar spectroscopic studies, SL domains were also implicated in binary PC/cholesterol bilayers.[1,7,17,21] Both saturated and unsaturated PC can participate in the SL domain formation in the PC/cholesterol system,[1,4,7] while mono-unsaturated PE and PC are involved in the PE/PC system. It is important to mention that sterol superlattice has been detected in a sterol/POPC/POPE ternary system by Wang et al.[42] Overall, the spectroscopically derived critical compositions match favorably with the critical compositions predicted by the Headgroup and Cholesterol SL models.

DPH-PC is an acyl-chain-labeled fluorescent PC whose structure resembles a saturated dipalmitoyl−PC. For X_{CHOL} < 0.60 in POPC/cholesterol bilayers, major dips at $X_{CHOL} \approx 0.40$ and 0.50 in steady-state anisotropy, fluorescent lifetime, and order parameter of DPH-PC in the POPC/cholesterol bilayer were reported.[17] These dips have been associated with the hypothesis that the DPH-PC probe partitions into the bilayer

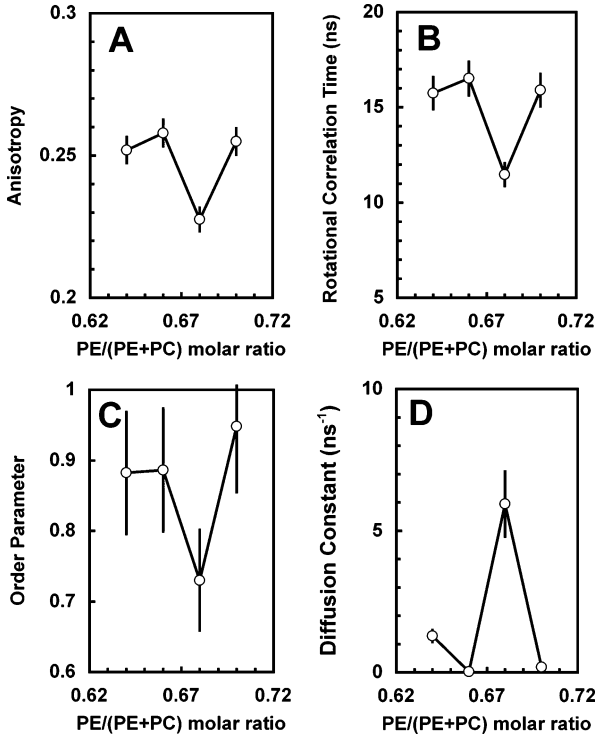

Figure 6. Time-resolved fluorescence anisotropy decay parameters of DPH-PC in POPE/POPC/CHOL bilayers as a function of X_{PE} at a fixed $X_{CHOL} = 0.40$. (A) Steady-state anisotropy, (B) rotational correlation time, (C) diffusion constant, and (D) order parameter are shown. The uncertainties of the fitted parameters obtained from three independent samples are indicated by error bars.

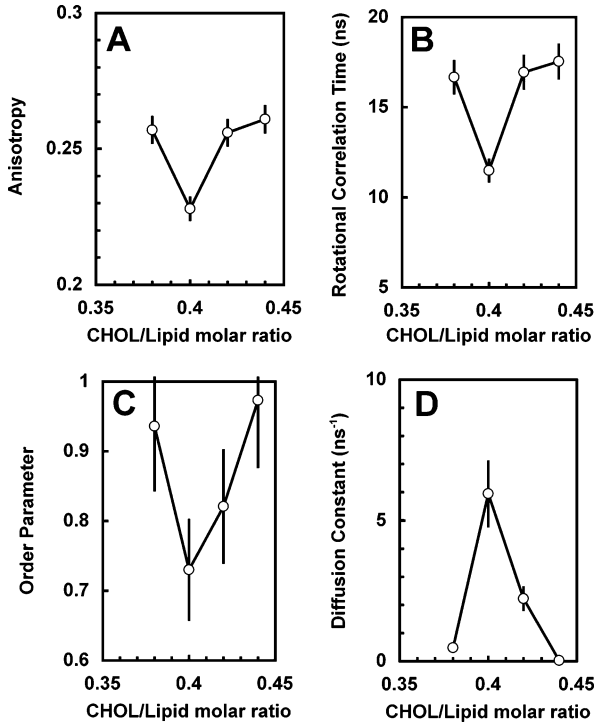

Figure 7. Time-resolved fluorescence anisotropy decay parameters of DPH-PC in POPE/POPC/CHOL bilayers as a function of X_{CHOL} at a fixed $X_{PE} = 0.68$. See the legend of Figure 6 for details.

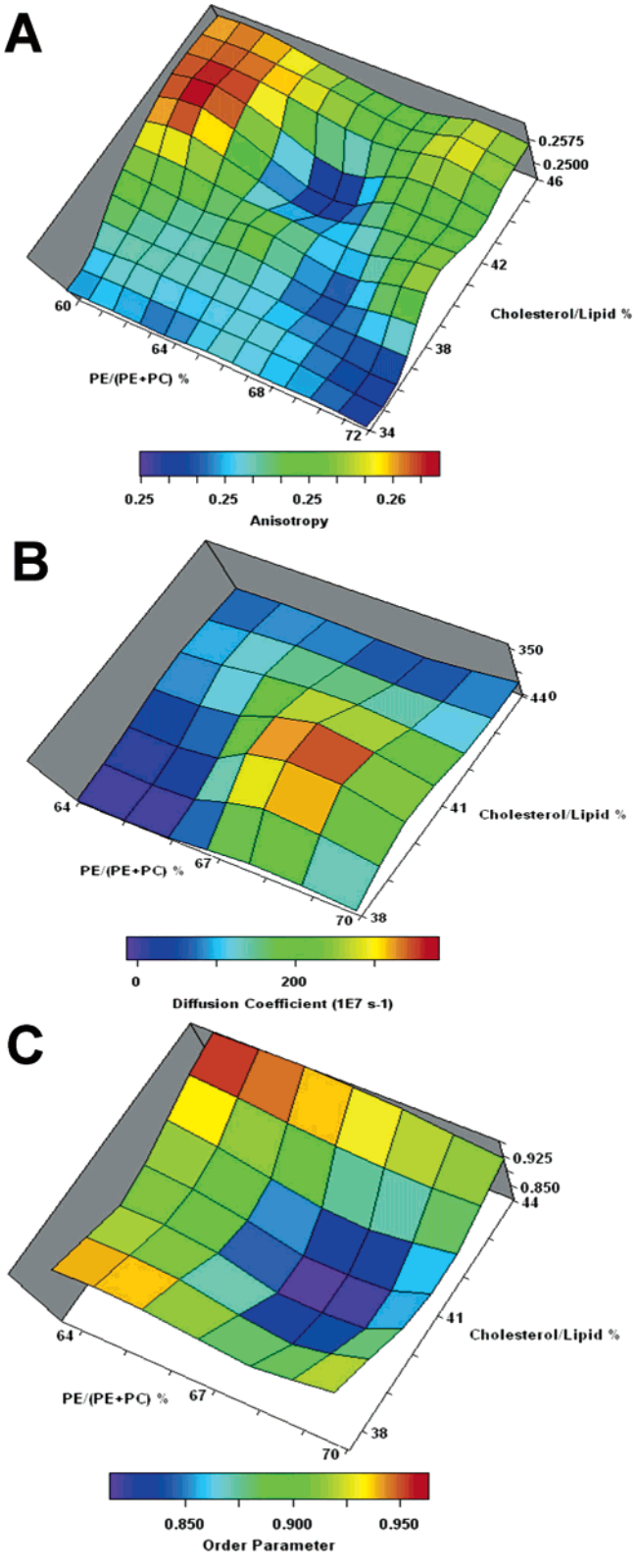

Figure 8. Three-dimensional surface plots of steady-state and time-resolved fluorescence parameters of DPH-PC in POPE/POPC/CHOL bilayers versus X_{PE} and X_{CHOL}. The surface plots of (A) steady-state fluorescence anisotropy, (B) order parameter, and (C) diffusion coefficient are shown. The fluorescence anisotropy plot represents measurements from four independently prepared ternary mixtures with systematically varying PE and cholesterol contents. Each sample set was equilibrated at 23 °C for at least 10 days after the preparation. See the Results section for details of the 3D surface plot generation. Surface plots of time-resolved fluorescence parameters of DPH-PC represent results from one of the three independently prepared ternary mixtures.

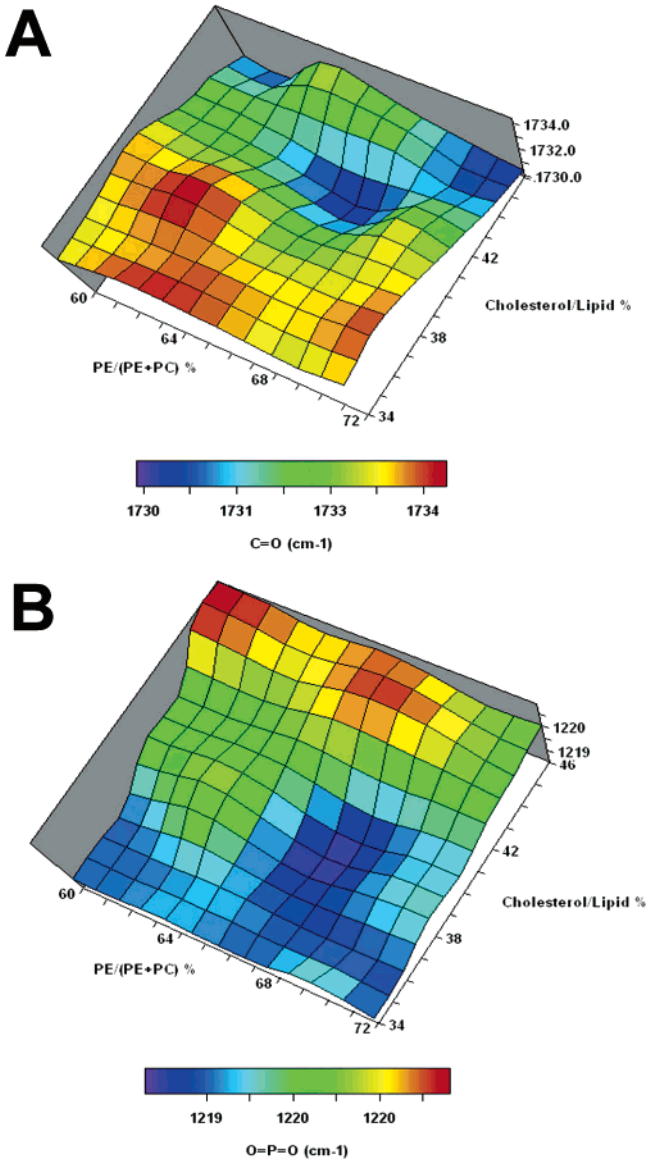

Figure 9. Three-dimensional surface plots of FTIR vibrational peak frequencies in POPE/POPC/CHOL bilayers versus X_{PE} and X_{CHOL}. The surface plots of (A) C═O peak frequency and (B) O═P═O peak frequency are shown. See the legend of Figure 8 for other details.

packing defect regions due to the unfavorable interaction of the bulky diphenylhexatriene conjugate of DPH-PC with cholesterol in the PC/cholesterol domains. In this respect, the fluorescence parameters of DPH-PC, both steady-state and time-resolved, would be useful to explore the existence of SL domains in POPE/POPC/cholesterol system, in which the single PC species in the PC/cholesterol system is replaced by the PE/PC binary mixtures of defined composition. For the PE/PC binary system, only dipyrenyl−PC (intramolecular excimer-forming molecule), Laurdan (membrane surface hydration/packing sensitive molecule), and dehydroergosterol (structural similar to cholesterol) probes have been used.[15,16] Whether or not DPH-PC is able to detect the SL domain formation in PE/PC or PE/PC/cholesterol was still unknown. This study demonstrates that DPH-PC probe is useful in investigating systematically the role of headgroup size difference and cholesterol content on the domain formation behavior in a monosaturated phospholipid/cholesterol system consisting of phospholipids of different headgroup sizes.

The gel-to-liquid crystalline phase transition temperature (T_m) of fully hydrated POPE or POPC bilayers are approximately

26 and 4 °C, respectively.[43,44] Our recent differential scanning calorimetry (DSC) data showed that POPE/POPC bilayers undergo a composition-driven transition at 23 °C from the liquid-crystalline state to the gel state when X_{PE} increases to ~0.85.[45] However, recent X-ray diffraction measurements on POPE bilayers revealed that T_m decreases from 25 to 10 °C upon inclusion of 20 mol % cholesterol, and no gel phase was evident at 35 mol % cholesterol.[46] Accordingly, the POPC/POPC/CHOL liposomal bilayers, at each composition used here, should be in the fluid state.

Table 1 summarizes the PE mole fractions at which deviations were observed at a fixed X_{CHOL} of 0.00, 0.35, 0.40, or 0.50 in the steady-state fluorescence anisotropy plots. When there was no cholesterol present, dips were observed at X_{PE} of 0.24, 0.34, 0.44, 0.49, 0.57, 0.67, 0.75, and 0.82. These compositions coincide with those obtained in previous studies using other fluorescent probes, i.e., Laurdan, dipyrenyl−PC, and dehydroergosterol.[15,16] Thus four structurally different fluorescent probes have revealed changes in the physical properties of the PE/PC bilayers at similar critical compositions. Except for X_{PE} of ~0.44 and 0.57, all these deviations agree with the critical compositions predicted by the Headgroup SL model,[1,6] supporting the presence of superlattice-like distributions of phospholipid headgroups in PE/PC bilayers. In the presence of cholesterol, deviations are still evident at several X_{PE}'s (Table 1). Among these, the ones at $X_{PE} \approx 0.33$ and 0.66 were consistently detected at each X_{CHOL}.

In the presence of 40 mol % cholesterol, FTIR measurements also revealed significant deviations at several X_{PE}'s (Table 2) coinciding with critical X_{PE}'s predicted by the Headgroup SL model. Significant deviations were again observed at $X_{PE} \approx 0.66$ for the C═O and O═P═O vibrations (Figure 3). These changes suggest that a significant increase in the conformational disorder and/or hydration at the lipid/water interface and phosphate headgroup region occurs near that critical composition.[17,31,45,47] Only a small peak or kink at $X_{PE} \approx 0.66$ was found for the C−H vibration, suggesting that a slight decrease in the ordering of the acyl chains may occur at that critical PE mole fraction. Note that more prominent peaks at $X_{PE} \approx 0.09$, 0.22, 0.31, 0.78−0.83, and 0.96 were observed in the C−H vibrational bands indicating reduction in the ordering of the acyl chains at those PE compositions.

Although headgroup SL domains at predicted critical PE mole fractions were detected in the presence of cholesterol, whether cholesterol SL domain and headgroup SL domain may coexist still awaited to be established. Since the steady anisotropy value contains the information for rotational dynamics, fluorescence intensity decay, and orientation, time-resolved fluorescence measurements were performed near the critical compositions of $X_{PE} \approx 0.68$. The dip in the fluorescence anisotropy at $X_{PE} \approx 0.68$ is associated with the decrease in the order parameter and an increase in the rotational diffusion constant of DPH. Similar conclusions were found for the dip at $X_{CHOL} \approx 0.40$ for a fixed $X_{PE} = 0.68$. The latter agreed with the results for DPH-PC in POPC/CHOL binary mixtures.[17] Here, $X_{CHOL} \approx 0.40$ corresponds to a critical cholesterol mole fraction for cholesterol SL formation as predicted by the cholesterol SL model.[1,7] Other critical cholesterol mole fractions for $X_{CHOL} \geq 0.10$ predicted by the cholesterol SL model are 0.100, 0.118, 0.125, 0.143, 0.154, 0.167, 0.182, 0.200, 0.222, 0.250, 0.286, 0.333, 0.500, and 0.667.[1,7,17]

The presence of "dips" in DPH-PC anisotropy and in C═O and O═P═O has been used as spectroscopic evidence for the confirmation of SL domain formation at both the headgroup and the acyl chain levels. It is believed that the fluorescent probe, DPH-PC, is sensing a more rotationally flexible and disordered environment at the critical compositions, e.g., $X_{PE} \approx 0.68$ and $X_{CHOL} \approx 0.40$. Most likely, DPH-PC partitions into the packing defect regions due to the less favorable interaction of its bulky DPH moiety with cholesterol in the putative SL domains.[17] Similarly, dips at the similar compositions were also detected by C═O and O═P═O, suggesting the critical increase in the compositional disorder and/or hydration at these two-dimensional critical compositions of PE and cholesterol. The probe-free FTIR measurements further support the existence of simultaneous superlattice-like distribution at the headgroup and acyl chain levels of fluid state lipid bilayers. Note that similar dips in DPH-PC and in C═O and O═P═O have been found in the binary POPC/CHOL binary mixtures.[17]

Although the presence of coexisting headgroup SL and cholesterol SL domains is implicated in this spectroscopic study, a visual inspection of the feasibility of those SL domains using a space filling representation may be required for some critical compositions. Figure 10 shows possible matches of one headgroup SL structure with CR symmetry with two tail group SL structures with CR and R symmetries that correspond to $X_{PE} = 0.67$ and $X_{CHOL}=0.40$. Here, PE and PC form headgroup SL structure with CR symmetry and with $(a, b) = (1, 1)$, or CR (1, 1). A representative CR unit cell consisting of two guest PC molecules and four PE host molecules is shown in Figure 10A. It is important to indicate that each PE or PC occupies two lattice sites at the acyl chain level in the cholesterol SL structure. Two possible cholesterol SL structures with CR (0, 2) and R (1, 2) are shown in Figures 10B and 10C. To match a total of 12 acyl chains from two PC and four PE molecules in a single CR (1, 1) unit cell of headgroup SL structure to the cholesterol SL structures at the acyl chain level, a ternary supercell containing exactly 12 lattice sites has to be found. In addition, one has to accommodate the two centrally located acyl chains originated from the guest PE molecule in the headgroup CR (1, 1) unit cell when they are mapped to the cholesterol SL structure at the acyl chain level. Therefore, offset units cells, i.e., cells with cholesterol shifts away from the center, have to be considered from the cholesterol SL structures at the acyl chain level. Here, ternary supercells consisting of two offset CR (0, 2) or four offset R (1, 2) unit cells can be constructed as shown in Figures 10B or 10C, respectively. Note that each ternary supercell contains four cholesterol molecules and 12 acyl chains and it provides a match for the corresponding PE and PC molecules at the headgroup level.

In this study as well as in our previous spectroscopic investigations of SLs,[15−17,21] not all predicted SL compositions were detected (Tables 1 and 2). This may be due to that the spectroscopic methods used are not sensitive enough to detect all predicted SL compositions and some SL domains may involve only subtle changes in the bilayer structures that evade detection by the current methods. Alternatively, some predicted compositions are just not stable enough to be detected. In addition, some deviations are observed at compositions that are not predicted by the current Headgroup SL model. These discrepancies indicate the existence of lipid domains that are not predicted by the current Headgroup or Cholesterol SL model, which is developed for a binary lipid system only. A new SL model that can explicitly describe the lateral organization of multiple lipid components at both the headgroup and the acyl chain levels is still needed.

The forces driving the lipid molecules toward regular, SL-like distributions have not been well established. In case of PC, the surface area occupied the strongly hydrated phosphocholine

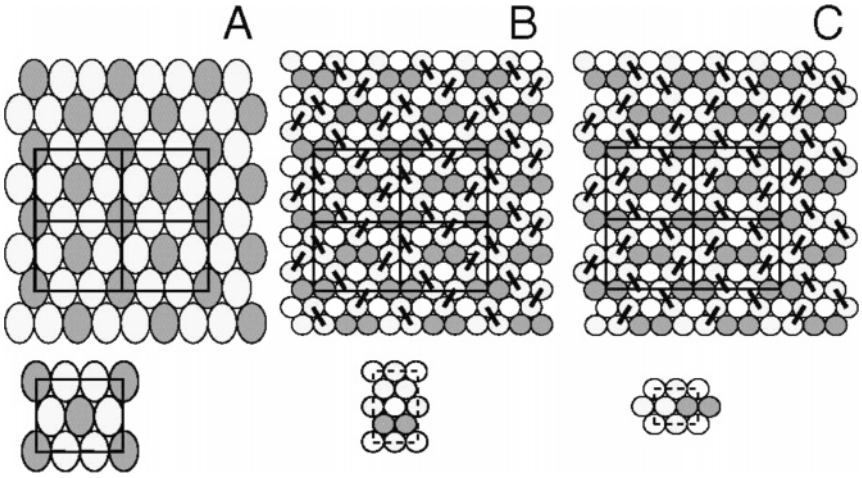

Figure 10. Molecular organizations of simultaneous superlattice domains at the headgroup and acyl chain levels at the theoretical critical compositions of $X_{PE} = 0.67$ and $X_{CHOL} = 0.40$. (A) The molecular organization of the lipid headgroups. The top figure shows a PE/PC headgroup superlattice composed of CR (1, 1) cells. PE host (light gray) and PC guest (dark gray) are shown at a ratio of 2:1 or 66 mol % PE and 33 mol % PC. The solid squares show four CR (1, 0) unit cells. A single CR (1, 0) unit cell is shown in the lower subfigure. Two different acyl chain superlattice structures can correspond to this headgroup arrangement. (B) A CR (1, 2) superlattice, in which two offset acyl chain unit cells match each headgroup unit cell. (C) A R (2, 0) superlattice, in which four offset acyl chain unit cells match each headgroup unit cell. For parts B and C, the host lipids are gray as in part A, and the guest cholesterol is shown as a white disk. At the acyl chain level there are four PE tails for each two PC tails, with the two acyl chains of each phospholipid shown connected by the dark bars. The unit cell of each acyl chain superlattice is shown by the dashed square in each subfigure.

headgroup of PC is probably larger than the cross-sectional area of the acyl chains. This imbalance leads to both rowding of the headgroup level and looser packing of the acyl chains as compared to lipids with headgroup and acyl chain cross-sectional area matching. When a lipid with a relatively small headgroup (e.g., cholesterol, diglyceride, or PE) is mixed with PC, the crowding at the headgroup region is relieved, and the packing (order) of the acyl chains increases. In the case of cholesterol, the rigid ring system of this lipid probably also contributes to this increased ordering of the acyl chains. Second, it is very likely that cholesterol also seeks to interact with PC since its headgroup (a single hydroxyl) is far too small to fully shield its hydrocarbon part from unfavorable contacts with water. This umbrella model is supported by both physical measurements as well as Monte Carlo simulations.[22,38,48] The spacer and umbrella effects are obviously maximal when the components are evenly (rather than randomly) distributed, which would make regular lateral distributions of cholesterol energetically more favorable than random ones.[1]

Although the physiological significance of SL domains in binary PC/CHOL or PE/PC bilayers has been implicated in recent studies,[4,41,42,45,49] the potential role of simultaneous headgroup and cholesterol SLs in membrane-related activities in ternary PE/PC/CHOL is still not clearly established. Our current results provide new physical insight into the structure of the lipid bilayer membrane, for compositions that approach those found in living systems. The spectroscopic evidence presented by this work, in conjunction with feasible structures, Figure 10, suggest that regular superlattice structures may coexist at both the headgroup and the acyl chain levels. This coexistence suggests the possibility of interactions between superlattices that result in increased overall structural stability. Furthermore, these coexisting structures take into account the steric requirements that the acyl chains be paired. Taken together with the steric implications of the umbrella model[38] and the ordering effect that the rigid cholesterol ring structure provides, it is not suprising that lipid composition is tightly controlled in biological systems[1,6,45] Future work in both experimental and theoretical areas of exploring the structural organization of lipid domains in this complex cholesterol−phospholipid system is urgently needed.

Acknowledgment. This work was supported by the Robert A. Welch Research Foundation grant (D-1158) to K.H.C., National Science Foundation grants to M.V. and J.H., and a grant from the Finnish Academy to P.S.

References and Notes

(1) Somerharju, P.; Virtanen, J. A.; Cheng, K. H. *Biochim. Biophys. Acta* **1999**, *1440*, 32.
(2) Simons, K.; Vaz, W. L. *Annu. Rev. Biophys. Biomol. Struct.* **2004**, *33*, 269.
(3) Simons, K.; Ikonen, E. *Science* **2000**, *290*, 1721.
(4) Chong, P. L.-G.; Olsher, M. *Soft Mater.* **2004**, *2*, 85.
(5) McConnell, H. M.; Radhakrishnan, A. *Biochim. Biophys. Acta* **2003**, *1610*, 159.
(6) Virtanen, J. A.; Cheng, K. H.; Somerharju, P. *Proc. Natl. Acad. Sci. U.S.A.* **1998**, *95*, 4964.
(7) Chong, P. L.; Sugar, I. P. *Chem. Phys. Lipids.* **2002**, *116*, 153.
(8) Simons, K.; Ikonen, E. *Nature* **1997**, *387*, 569.
(9) Mukherjee, S.; Zha, X.; Tabas, I.; Maxfield, F. R. *Biophys. J.* **1998**, *75*, 1915.
(10) Feigenson, G. W.; Buboltz, J. T. *Biophys. J.* **2001**, *80*, 2775.
(11) Leidy, C.; Wolkers, W. F.; Jorgensen, K.; Mouritsen, O. G.; Crowe, J. H. *Biophys. J.* **2001**, *80*, 1819.
(12) Anderson, R. G.; Jacobson, K. *Science* **2002**, *296*, 1821.
(13) London, E. *Curr. Opin. Struct. Biol.* **2002**, *12*, 480.
(14) Ramstedt, B.; Slotte, J. P. *FEBS Lett.* **2002**, *531*, 33.
(15) Cheng, K. H.; Virtanen, J.; Somerharju, P. *Biophys. J.* **1999**, *77*, 3108.
(16) Cheng, K. H.; Ruonala, M.; Virtanen, J.; Somerharju, P. *Biophys. J.* **1997**, *73*, 1967.
(17) Cannon, B.; Heath, G.; Huang, J.; Somerharju, P.; Virtanen, J. A.; Cheng, K. H. *Biophys. J.* **2003**, *84*, 3777.
(18) Parente, R. A.; Lentz, B. R. *Biochemistry* **1985**, *24*, 6178.
(19) Chen, S. Y.; Cheng, K. H. *Biophys. J.* **1996**, *71*, 878.
(20) Cheng, K. H. *Biophys. J.* **1989**, *55*, 1025.
(21) Parker, A.; Miles, K.; Cheng, K. H.; Huang, J. *Biophys. J.* **2004**, *86*, 1532.
(22) Huang, J.; Feigenson, G. W. *Biophys. J.* **1999**, *76*, 2142.
(23) Kingsley, P. B.; Feigenson, G. W. *Chem. Phys. Lipids* **1979**, *24*, 135.
(24) Gratton, E.; Jameson, D. M.; Hall, R. D. *Annu. Rev. Biophys. Bioeng.* **1984**, *13*, 105.
(25) James, D.; Siemiarczuk, A. *Rev. Sci. Instrum.* **1992**, *63*, 1710.

(26) Lakowicz, J. R.; Laczko, G.; Cherek, H.; Gratton, E.; Limkeman, M. *Biophys. J.* **1984**, *46*, 463.
(27) Van der Meer, B. W.; Cheng, K. H.; Chen, S. Y. *Biophys. J.* **1990**, *58*, 1517.
(28) Chen, S. Y.; Cheng, K. H.; Van der Meer, B. W.; Beechem, J. M. *Biophys. J.* **1990**, *58*, 1527.
(29) Perrin, F. *J. Phys. Radium.* **1936**, *71*, 1.
(30) Cheng, K. H. *Chem. Phys. Lipids.* **1994**, *70*, 43.
(31) Kodati, V. R.; Lafleur, M. *Biophys. J.* **1993**, *64*, 163.
(32) Pare, C.; Lafleur, M. *Biophys. J.* **1998**, *74*, 899.
(33) Savitzky, A.; Golay, M. J. E. *Anal. Chem.* **1964**, *36*, 1627.
(34) Whittaker, E. T.; Robinson, G. *Graduation, or the Smoothing of Data*, 4th ed.; Dover: New York, 1967.
(35) Ferguson, G. A. *Statistical Analysis in Psychology and Education*, 3rd ed.; McGraw-Hill: New York, 1971.
(36) Cheng, K. K.; Thacker, B. A.; Cardenas, R. L.; Crouch, C. *Am. J. Phys.* **2004**, *72*, 1447.
(37) Martin, R. B.; Yeagle, P. L. *Lipids* **1978**, *13*, 594.
(38) Huang, J. *Biophys. J.* **2002**, *83*, 1014.
(39) Cardenas, R. L.; Cheng, K. H.; Verhey, L. J.; Xia, P.; Davis, L.; Cannon, B. *Magn. Reson. Imaging* **2002**, *20*, 667.
(40) Simons, K.; van Meer, G. *Biochemistry* **1988**, *27*, 6197.
(41) Liu, F.; Chong, P. L. *Biochemistry* **1999**, *38*, 3867.
(42) Wang, M. M.; Sugar, I. P.; Chong, P. L. *Biochemistry* **1998**, *37*, 11797.
(43) Barenholtz, Y.; Suurkuusk, J.; Mountcastle, D.; Thompson, T. E. *Biochemistry* **1976**, *15*, 2441.
(44) Small, D. M. *The Physical Chemistry of Lipids*; Plenum Press: New York, 1986.
(45) Cannon, B.; Hermansson, M.; Gyorke, S.; Somerharju, P.; Virtanen, J. A.; Cheng, K. H. *Biophys. J.* **2003**, *85*, 933.
(46) Wang, X.; Quinn, P. J. *Biochim. Biophys. Acta* **2002**, *1564*, 66.
(47) Lafleur, M.; Cullis, P. R.; Bloom, M. *Eur. Biophys. J.* **1990**, *19*, 55.
(48) Huang, J.; Buboltz, J. T.; Feigenson, G. W. *Biochim. Biophys. Acta* **1999**, *1417*, 89.
(49) Wang, M. M.; Olsher, M.; Sugar, I. P.; Chong, P. L. *Biochemistry* **2004**, *43*, 2159.